Current advances on Talbot-Lau X-Ray Imaging Diagnostics for High Energy Density experiments

M. P. Valdivia[1,2,a)], G. Perez-Callejo[3], V. Bouffetier[4], G. W. Collins IV[5], C. Stoeckl[6], T. Filkins[6], C. Mileham[6], M. Romanofsky[6], I. A. Begishev[6], W. Theobald[6], S. R. Klein[7], M. K. Schneider[8], F. N. Beg[1], A. Casner[9], D. Stutman[10]

[1]*Center for Energy Research, University of California San Diego, La Jolla, California 92093, USA*
[2]*Physics and Astronomy Department, The Johns Hopkins University, Baltimore, Maryland 21218, USA*
[3]*Departamento de Física Teórica, Atómica y Óptica, Universidad de Valladolid, 47011 Valladolid, Spain*
[4]*European XFEL GmbH, Holzkoppel 4, 22869 Schenefeld, Germany*
[5]*General Atomics, Inertial Fusion Technology, San Diego, California 92121, USA*
[6]*Laboratory for Laser Energetics, University of Rochester, Rochester, New York 14623, USA*
[7]*University of Michigan, Ann Arbor, Michigan 48109, USA*
[8]*Johns Hopkins University, Applied Physics Laboratory, Laurel, Maryland 20723, USA*
[9]*CEA-CESTA, 15 avenue des Sablières, CS 60001, 33116 Le Barp CEDEX, France*
[10]*ELI-NP, Institute for Physics and Nuclear Engineering, Bucharest-Magurele 077125, Romania*

[a)]Author to whom correspondence should be addressed: mpvaldivialeiva@ucsd.edu.

(Presented XXXXX; received XXXXX; accepted XXXXX; published online XXXXX)
(Dates appearing here are provided by the Editorial Office)

Talbot-Lau X-ray Interferometry is a refraction-based diagnostic that can map electron density gradients through phase-contrast methods. Talbot-Lau X-ray Deflectometry (TXD) diagnostics have been deployed in several High Energy Density experiments. To improve diagnostic performance, a monochromatic TXD was implemented on the Multi-Tera Watt (MTW) laser using 8 keV multilayer mirrors ($\Delta\theta/\theta$ = 4.5-5.6%). Copper foil and wire targets were irradiated at $10^{14\text{-}15}$ W/cm^2. Laser pulse length (~10-80 ps) and backlighter target configurations were explored in context of Moiré fringe contrast and spatial resolution. Foil and wire targets delivered increased contrast < 30%. The best spatial resolution (<6 μm) was measured for foils irradiated 80° from the surface. Further TXD diagnostic capabilities enhancement was achieved through the development of advanced data postprocessing tools. The Talbot Interferometry Analysis (TIA) code enabled x-ray refraction measurements from MTW monochromatic TXD. Additionally, phase, attenuation, and dark-field maps of an ablating x-pinch load were retrieved through TXD. The images show a dense wire core of ~60 μm diameter surrounded by low-density material of ~40 μm thickness with an outer diameter ratio of ~2.3. Attenuation at 8 keV was measured at ~20% for the dense core and ~10% for the low-density material. Instrumental and experimental limitations for monochromatic TXD diagnostics are presented. Enhanced postprocessing capabilities enabled by TIA are demonstrated in context of high-intensity laser and pulsed power experimental data analysis. Significant advances on TXD diagnostic capabilities are presented. These results inform future diagnostic technique upgrades which will improve the accuracy of plasma characterization through TXD.

I. INTRODUCTION

The advent of mid-scale high-intensity and ultra-fast lasers, pulsed power current drivers, and combinations thereof, has enabled high energy density plasma (HEDP), x-ray and laser-matter interaction, and warm dense matter studies [1]. These facilities provide a wide variety of experimental platforms to study new physics regimes and thus, are fundamental for developing diagnostics that can properly characterize these new regimes.

Talbot X-ray Interferometry in HEDP experiments

X-ray imaging is a powerful tool that can deliver immediate experimental feedback in real-time in addition to providing useful information from data post-processing. In view of this, an x-ray refraction imaging diagnostic has been developed to characterize HEDP experiments built upon medical and biological research applications [2], [3]. Talbot-Lau X-ray Interferometry has been used to infer electron density gradients in matter by measuring the angular deflection of x-rays that pass through the material [4], [5], surpassing attenuation-based x-ray imaging techniques due to the inherent contrast enhancement in refraction signatures for low-Z matter probed at energies <100 keV [6]. In the Talbot X-ray Deflectometry (TXD)

mode [7], phase, attenuation, and dark-field information can be retrieved simultaneously from a single Moiré image through Fourier methods. In addition to electron density gradient mapping, TXD can provide material mixing information by combining attenuation and refraction signals [8] as well as detect micro-structures due to instabilities through small-angle x-ray scattering measurements. Furthermore, ex-situ reference images can be obtained through phase-stepping methods [9], thus enabling single-shot diagnostics.

To enhance x-ray imaging diagnostic capabilities in HED environments, TXD diagnostics have been deployed at several HED facilities [10]–[15]. Dedicated TXD diagnostic platforms have been benchmarked at the Laboratory for Laser Energetics (LLE) for the Multi-TeraWatt (MTW) [16] and OMEGA-EP lasers, the GenASIS Linear Transformer Driver (LTD) at the University of California San Diego [17], and most recently at the X-Ray Free Electron Laser (XFEL) facility SACLA. While these experiments have successfully demonstrated x-ray refraction angle and electron density retrieval, the optimization of x-ray backlighters for Talbot Interferometry remains a challenge [15]. Specifically, the bandwidth of the interferometer design energy and x-ray backlighter spectra impact imaging contrast. Talbot interferometer contrast is determined by the so-called interferometer contrast curve, which factors in grating periods and composition as well as interferometer parameters such as Talbot distances, order, and magnification [6]. Since Moiré fringe contrast optimization is paramount to electron density measurement accuracy, monochromatic x-ray backlighting matching the interferometer design energy optimizes TXD diagnostic performance. Moreover, broadband x-ray emission reduces signal-to-noise-ratio (SNR) along with interferometer. Consequently, spatial resolution is also degraded, which further hinders the overall TXD diagnostic performance.

The present manuscript presents recent advances on TXD diagnostic methods. Using a graded multilayer mirror, a monochromatic variation of the diagnostic was implemented in the high-intensity laser environment. Experiments were conducted to systematically study diagnostic performance. Advanced numerical tools have been implemented, improving TXD data postprocessing methods and enabling accurate single-shot retrieval of x-ray phase, attenuation, and dark-field maps of samples relevant to HED research. The remainder of the manuscript is as follows: Sec. 2 provides background information on standard and monochromatic TXD diagnostics. Sec. 3 describes the implementation and diagnostic performance characterization of monochromatic TXD in the high-intensity laser environment. Sec. 4, presents x-ray images obtained with TXD diagnostics and postprocessing with the dedicated Talbot Interferometry Analyzer (TIA) tool [18]. Experimental x-ray refraction profiles are compared with simulations in the case of monochromatic TXD images recorded using x-ray backlighting from a high-intensity laser. TXD images from an expanding wire x-pinch load, recorded using laser-cut x-pinch backlighting [12], are presented along with x-ray phase, attenuation, and dark-field maps retrieved through TXD methods.

II. MONOCHROMATIC TXD DIAGNOSTICS

Monochromatic x-ray emission has been used to characterize a wide array of HEDP systems through x-ray imaging diagnostics. In these experiments, monochromatic x-ray backlighting was obtained from polychromatic sources by using specialized crystals [19]–[23]. While well-established, these techniques are susceptible to imaging aberrations due to imperfect crystal surfaces, which are especially detrimental to Talbot-Lau x-ray interferometry diagnostics. Considering instrumental restrictions from the specific system to be deployed, the ideal x-ray reflector for TXD diagnostics is a multilayer mirror reflecting a narrow energy range in a single direction [24]. Moreover, multilayer mirrors have been used to diagnose HEDP plasmas [25], [26], albeit using propagation-based x-ray imaging methods.

A. Laterally graded multilayer mirror

At normal incidence, x-rays and extreme ultraviolet beams (λ ~0.1-500 Å) can easily penetrate most materials while being strongly absorbed by other materials. In contrast, at glancing or grazing incidence, total beam reflection can be maximized. Recall that x-ray reflection against a crystal surface occurs only for the wavelengths that satisfy by Bragg's Law:

$$m\lambda = 2d\,\sin\theta, \tag{1}$$

where λ and θ are the wavelength and incidence angle of the incoming x-ray beam, respectively, d is the distance between two adjacent layers of the atomic crystal structure, and m is an integer.

Even if Bragg's law is satisfied, only a small portion of the x-ray beam will be reflected, while most of the beam will be refracted and propagate further into the material. Nevertheless, incoming beam reflection can be optimized through coherent addition of multiple reflections. Multilayer mirrors make use of this by combining laterally graded thin planar layers of two different materials. The index of refraction and thickness of the layers are chosen such that at each interface, Bragg reflection will occur at one specific wavelength.

For an x-ray point source, peak reflectivity only occurs at the specific location along the mirror length where the incidence angle satisfies Bragg's Law. In contrast to crystals, graded multilayer mirrors are composed of layers with thickness that vary continuously along the mirror length. Thus, Bragg's Law is satisfied for a single

wavelength despite changing beam angle of incidence along the mirror, as illustrated in Figure 1.

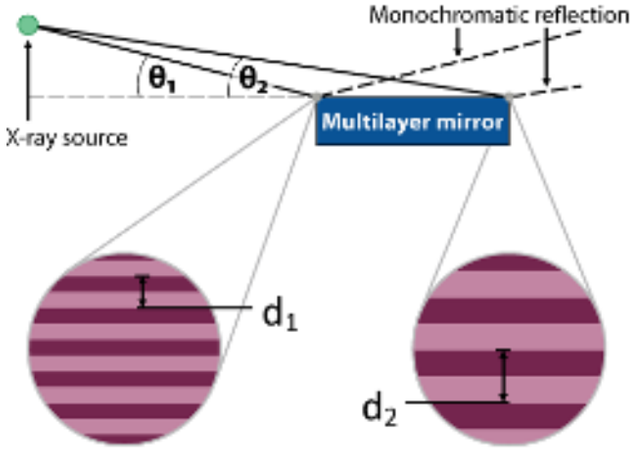

FIG. 1. Schematic of a multilayer mirror. The x-ray energy reflected follows Bragg's Law, which is satisfied at all points of the mirror surface through layer thickness variation to conserve the refraction angle relative to the x-ray source.

B. Monochromatic TXD diagnostic for the MTW laser

The standard TXD diagnostic platform used previously on the MTW laser was re-designed to establish Monochromatic TXD (M-TXD) diagnostics [10], [15]. Laterally graded multilayer mirrors were integrated to the Talbot-Lau X-ray Interferometer standard design. Consequently, the x-ray source, gratings, and detector orientation were modified to match the new diagnostic line-of-sight (LOS). The MTW monochromatic TXD diagnostic rail is shown in Figure 2.

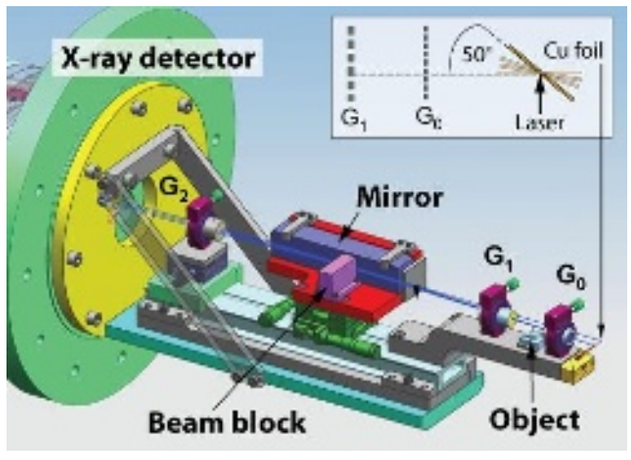

FIG. 2. MTW monochromatic TXD diagnostic rail drawings showing backlighter target, gratings, mirror, beam block, object, and detector locations. The inset shows the different laser incidence angles (with respect to diagnostic LOS) tested in the experiments.

The newly implemented MTW M-TXD diagnostic rail (Figure 2) incorporates a laterally-graded multilayer mirror with alternating tungsten and boron carbide multilayer structures and a 100 x 20 mm reflecting surface. The mirrors were designed for optimal reflection of Cu K_α emission at 8.05 keV considering mirror and x-ray source location in the laser vacuum chamber. Layer d-spacing increases from d_1 = 15.3 Å (mirror edge closest to the x-ray source) to d_2 = 24.8 Å (mirror edge closest to the detector). With a bandwidth of $\Delta\theta/\theta \approx 4.93\%$, optimal reflection is achieved at $\theta_1 = 2.884°$ and $\theta_2 = 1.779°$ ($\Delta\theta/\theta$ = 4.53% and 5.59%, respectively). A beam block was added to prevent stray radiation from reaching the detector. The mirror was placed in between the phase (G_1) and analyzer (G_2) gratings to prevent damage due to proximity to the laser. A 25 µm Mylar filter was placed in front of the source grating (G_0) to mitigate laser-induced damage.

As in previous MTW experiments [5], [6], [10], [15], copper targets were irradiated at intensities of ~$10^{14\text{-}15}$ W/cm^2 to obtain x-ray backlighting from Cu K_α emission at ~8 keV. Planar foils of 500 x 500 x 20 µm^3 were irradiated at approximately 50°, 70°, 80°, and 90° from target surface, as shown in Figure 2. Wires of 20 µm diameter were also tested. To further analyze the effect of laser pulse length on the production of high energy emission due to hot electron recirculation, photon flux and x-ray spectra were analyzed for laser pulses of ~10-80 ps at 22-36 J.

C. Monochromatic Moiré images

Monochromatic Moiré images were recorded using an x-ray charged-coupled device (CCD) with a 25 µm Mylar filter at an object magnification of ~8.5. Copper grids with a 127 µm pitch were imaged using the monochromatic TXD diagnostic especially designed for the MTW laser system.

1. Laser pulse length variation at I ~10^{14} W/cm^2

Table 1 presents Moiré fringe contrast, SNR, and relative x-ray CCD counts obtained from sets of M-TXD images. Cu foils were irradiated at 50° using three different laser configurations. Standard (non-monochromatic) TXD data from previous experiments are also provided for comparison.

TABLE I. M-TXD Moiré parameters obtained for three laser pulse lengths and standard TXD parameters for a matching laser pulse length.

Laser pulse length (ps)	Intensity (10^{14} W/cm^2)	SNR	Contrast (%)	Relative counts
25 (at 27 J)	7.3	6.0-7.9	24-25	1
60 (at 36 J)	4.1	6.9-7.2	21-24	1.30
80 (at 29 J)	2.5	6.0-8.6	27-30	0.71
Standard TXD				
24 (at 27 J)	4.4	3.5	19	1.85

When comparing results from monochromatic TXD to standard TXD, all laser pulse lengths explored showed higher Moiré fringe contrast (21-30%). Notably, for equivalent pulse length or intensity, SNR values are nearly doubled. While relative x-ray CCD counts are higher for standard TXD diagnostics, the lower Moiré fringe contrast measured in this configuration (19%) demonstrates that a significant amount of these counts are due to emission from sources other than Cu K_α emission. This demonstrates that monochromatic x-ray backlighting significantly improves TXD diagnostic performance. In the results presented, Moiré fringe contrast approaches the maximum value theoretical value expected (~35%) for this particular Talbot-Lau interferometer configuration.

Further, a relative photon count increase is observed for 25 versus 60 ps laser pulse length, which is accompanied by a lower Moiré fringe contrast. This indicates that sources other than Cu K_α emission contribute to the contrast reduction considering higher laser energy for the 60 ps pulse length. Conversely, when comparing data for 25 and 80 ps, a longer laser pulse length results in a slightly lower photon flux. Nevertheless, they favor monochromatic emission at 8 keV, as evidenced by increased contrast, even at slightly higher laser energies. Considering the above, future experiments will further investigate the effect of laser pulse length on monochromatic TXD diagnostics regarding Moiré contrast and flux recorded at the detector using a constant laser intensity value.

2. Target type variation: Planar foils and wires

Previously, it was demonstrated that TXD diagnostic spatial resolution was increased when using so-called micro-backlighter targets, such as wires, spheres, and bookends. The x-ray source size reduction was also observed for planar foil targets irradiated normal to the surface [15]. However, these target schemes showed increased higher energy emission, which was detrimental to Moiré fringe contrast. Monochromatic TXD was deployed at the MTW laser in combination with wire backlighter targets. Relative x-ray backlighter quality was evaluated for wire and foil targets at two different laser incidence angles.

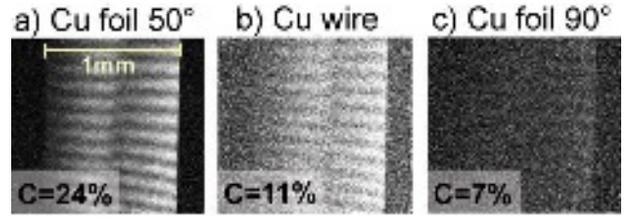

FIG. 3. M-TXD Moiré from three backlighter target configurations: a) Cu foils irradiated at 50°, b) Cu wires, and c) Cu foils irradiated at 90°. Note that the color contrast from the Moiré images shown has been enhanced to better showcase Moiré fringes.

Moiré images (Fig. 3) were obtained through M-TXD diagnostics using three backlighter target configurations irradiated at I ~4 x 10^{14} W/cm^2 (36 J, 57 ps). These images correspond to the x-ray CCD camera full chip (~1.3 x 1.3 mm^2). In the monochromatic TXD mode, the effective field-of-view is restricted to ~68% in the horizontal (density gradient detection) direction due to the multilayer mirror length. Note that the "broken fringes" observed in the middle of the image are due to source grating imperfections rather than refraction effects. The implications of grating structure imperfections have been discussed previously [5].

Figure 3 confirms that Cu foils irradiated at 50° deliver the highest Moiré fringe contrast at 24% with SNR = 6.9. In turn, with similar detector counts and SNR = 1.9, Moiré fringe contrast for Cu wires was 11%. Previously published results from standard TXD diagnostic measurements on the MTW laser support a reduction in Moiré fringe contrast for wire targets in comparison to foil targets. Note that a Cu K_α conversion efficiency of ~3 x 10^{-5} has been measured for foils irradiated at I ~ $10^{14\text{-}15}$ W/cm^2 on MTW. This value is about 3 times larger than the ~9 x 10^{-6} conversion efficiency obtained with wire targets, which is similar to their SNR ratio. Overall, additional data are needed to better determine suitability of wire targets as x-ray backlighters for M-TXD diagnostics.

On the other hand, Cu foils irradiated at 90° delivered an even lower contrast of 7% with much-reduced SNR of 1.2. When compared to 50° foil orientation, detector counts were reduced to ~20% of the expected values. This is not consistent with Cu K_α conversion efficiency measurements, hence, there must be an additional factor at play that restricts monochromatic emission from reaching the detector.

While the implementation of a multilayer mirror might appear to be straight forward from a mechanical point of view, several system limitations arise from this addition. In the case of the MTW monochromatic TXD diagnostic rail, it has been found that mirror positioning requires a mirror alignment precision of ~0.015°. This translates to extremely sensitive backlighter target alignment with respect to diagnostic LOS. In the MTW laser system, laser intensity can be changed by varying laser spot size, achieved through backlighter target defocusing. For example, if the target is moved towards the laser beam by about 90 μm, the laser

intensity on target can be roughly reduced by a factor of 2. While this does not impact standard TXD diagnostics significantly, the monochromatic TXD system here presented is extremely sensitive to displacements from diagnostic LOS. Using the numbers in the example above, the angle from x-ray source to mirror surface at the beam block location would change from 2.333° to 2.308° with a target displacement of ~90 μm, which is well above the 0.015° alignment precision.

While x-ray emission from foil targets irradiated at 50° is assumed to propagate towards the mirror unobstructed, emission from targets irradiated at 90° is obstructed by the foil target itself. In cases where laser intensity changes are required, backlighter target defocusing further reduces the effective reflection of x-rays as the foil is displaced away from the mirror surface towards the beam block. Moreover, if "edge-on" x-ray emission (as observed from the diagnostic LOS) is highly directional, this would prove to be an additional factor reducing total x-ray radiation reflected by the mirror. Note that x-rays emitted by wire targets are also unobstructed, albeit limited by the amount of material irradiated along the length of the wire.

3. Spatial resolution optimization through foil orientation

From results presented thus far, planar foil targets irradiated at 50° deliver the highest overall Moiré fringe contrast, photon flux, and SNR for the monochromatic TXD diagnostic platform deployed on the MTW laser. This is consistent with published data from standard (non-monochromatic) TXD diagnostics [15]. In this work, it was shown that spatial resolution >10 μm can limit the diagnostic accuracy. This study showed an improved spatial resolution of 3 μm for foil targets irradiated at 90°. Note that for the TXD diagnostic here described [6], the system spatial resolution is limited by the x-ray source size in combination with effective detector pixel size. Additionally, spatial resolution is directly related to target orientation and target dimension [27].

To investigate monochromatic TXD system spatial resolution, a systematic study was performed by irradiating foil targets at different angles of incidence, as shown in Figure 2 inset. Figure 4 shows the results obtained for 50°, 70°, and 80° angles of incidence.

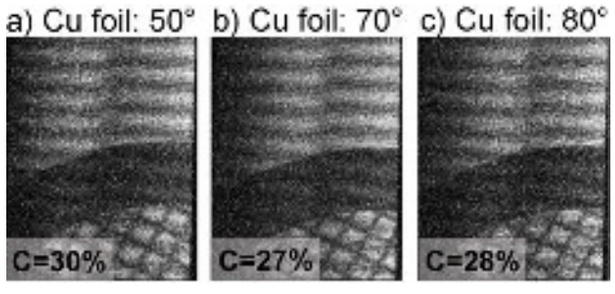

FIG. 4. A copper grid was imaged with the monochromatic TXD diagnostic designed for the MTW laser. The Moiré images were recorded using x-ray emission from planar foil backlighter targets irradiated at: a) 50°, b) 50°, and c) 80°. Note that color levels have been modified at scale to better showcase relevant features.

Consistent with results shown above, high Moiré fringe contrast was measured for all laser incidence angles tested at intensities of ~3 x 10^{14} W/cm^2 (29 J, 84 ps). It should be noted that detector photon count was consistent for all Moiré images shown in Figure 4. System spatial resolution was determined through knife edge-method considering 8 keV transmission through the copper grid. Spatial resolution was measured obtaining ~10.1 μm for foils irradiated at 50°, ~7.6 μm for 70°, and ~5.6 μm for 80°. Since spatial resolution measurements were limited to 5.5 μm by detector effective pixel size, it was determined that target irradiation at 80° is an adequate compromise between spatial resolution and x-ray flux optimization.

III. ADVANCED TXD PHASE-RETRIEVAL METHODS

The implementation of a Talbot-Lau Interferometry Analysis tool [18] represents a significant advancement to the TXD diagnostic technique. Interferometry has shown to be a valuable diagnostic for plasmas due to high sensitivity and accuracy [28]. However, few diagnostics have demonstrated feasibility using x-ray probing beams [29]–[31], which would effectively enable the characterization of higher plasma densities. One such diagnostic is the Talbot-Lau X-ray Deflectometer here presented. In the above, improvements to the TXD technique focused on instrument design and experimental variables. In this section, advances in TXD data postprocessing methods will be described.

TIA is a forward model capable of simulating Talbot and Talbot-Lau x-ray interferometry images. While similar tools exist, such as the IDL-based X-ray Wave Front Propagation (XWFP) code [32], the TIA code has proven to be a powerful addition to the TXD diagnostic technique that enables proper experimental design. TIA can produce synthetic Moiré images from a complete set of user-specified instrumental parameters. Moreover, the code can support complex plasma system modelling achieved by integrating output from hydrodynamic simulations.

Further, the Talbot Numerical Tool (TNT) -which is the postprocessing module of TIA- provides both experimental and synthetic interferometry image postprocessing. The tool was first used in feasibility studies of Talbot-Lau phase-contrast imaging using a high-intensity high-repetition-rate laser to obtain K_α x-ray sources [14]. A wealth of interferometry analysis codes is currently available to the HEDP community. For example, IDEA [33] is widely used by the pulsed power community in visible laser interferometry analysis. Still, none of these codes provide simultaneous phase, attenuation, and dark-field image retrieval suitable for TXD diagnostics. This capability is

important since small-angle scattering [34] can be inferred from dark-field images. Accurate detection of sub-resolution x-ray scattering information is a challenge for current x-ray imaging methods. These rely heavily on x-ray propagation effects, which are weak for the x-ray probing energies available in most HED experimental platforms. In turn, TXD methods provide independent attenuation and phase information from a single image. Moreover, plasma composition or mixing [8] can be inferred by combining this information. Note that preliminary comparisons between TIA and other interferometry analysis tools have shown that TIA surpasses phase retrieval accuracy while overcoming most common code limitations. These results will be presented in a future publication.

A. X-ray refraction retrieval: Monochromatic TXD

Monochromatic TXD images of a 500 μm diameter plastic (polymethyl methacrylate) rod are shown in Figure 5. The rod outline is provided in Figure 5 d). Additionally, one of the imperfections from the source grating is highlighted in Figure 5 e) for clarity. These TXD images were recorded on MTW using Cu K_α x-ray backlighting produced by laser-irradiating foil targets with intensities of ~3 x 10^{14} W/cm^2 at an angle of 50°.

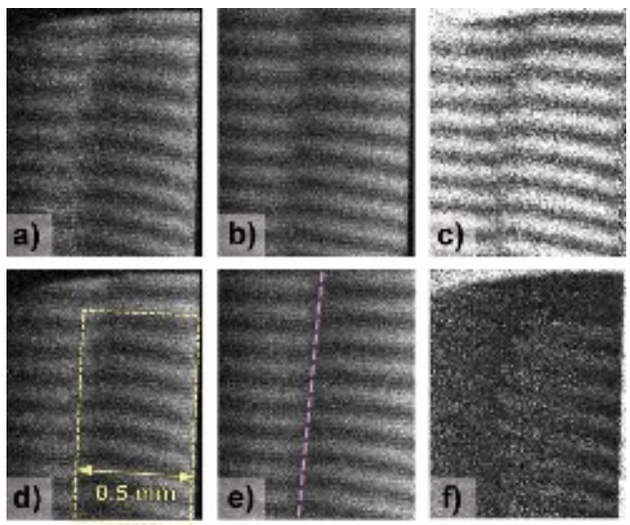

FIG. 5. Moiré images from the MTW M-TXD diagnostic. a, d) Images show a plastic rod (yellow dotted line in (d)) recorded with a laser pulse of ~36 J, 70 ps, b) Reference image from a 36 J, 60 ps laser pulse. C) Differential image showing object/reference (a) and b)) mismatch due to Moire fringe displacement. e) A dashed line highlights fringe "breaks" due to source grating structural imperfections (as observed in Figure 3). This reference image has been displaced vertically and horizontally to better match Moire fringes with the TXD rod image. f) Differential image between better matched object/reference images (d) and e)). Note that color levels have been modified to better showcase relevant features.

In these experiments, matching reference Moiré images were not available through experimental acquisition or ex-situ phase-stepping methods [9]. Nevertheless, through correlation methods, a reference image was selected from a set of images recorded using different laser backlighting parameters. Phase retrieval was enabled following backlighter background removal which delivered the x-ray refraction angle profile shown in Figure 6. It should be noted that the backlighter background removal feature was included in TNT considering data acquisition limitations in most HEDP experiments. It allows for postprocessing using reference images recorded with different x-ray sources.

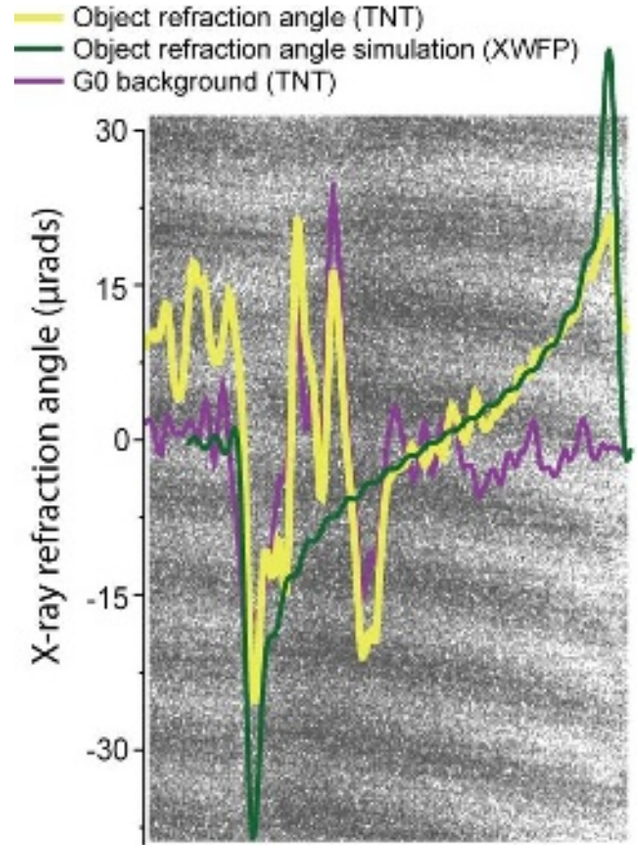

FIG. 6. Plastic rod monochromatic Moiré image. The respective x-ray refraction angle profile retrieved with TNT is shown along a simulated profile and the reference image "phase-background" expected due to source grating imperfections.

Figure 6 shows the x-ray refraction angle profile obtained through TNT along with the reference image, which was obtained using a flat field background. These results demonstrate that, in this case, grating imperfections are significant enough to prevent accurate phase retrieval in the "broken fringes" section. Nevertheless, outside this area, the x-ray refraction angle profile matches XWFP simulations within experimental error values. Note that a phase map could not be retrieved through IDEA when using the same input image used for TNT processing. This further supports the notion that the TIA code, along with its TNT module, represent an important advancement for TXD diagnostic techniques, hinting at advantages of TNT use for interferometry analysis of pulsed power experiments.

B. Wire x-pinch core expansion: phase, attenuation, and dark-field image retrieval through TXD

TXD diagnostic feasibility has been demonstrated previously in the pulsed power environment [13]. To optimize x-ray source quality for 8 keV TXD applications, a ~200 kA, 150 ns LTD was used to drive wire, hybrid [35] and laser-cut [36] x-pinch loads [37]. It was found that Cu K_α emission reproducibility is higher for laser-cut x-pinch loads when compared to wire and hybrid x-pinches. Moreover, laser-cut copper x-pinches produced bright sources ($<10^6$ W peak power) ideal for 8 keV TXD imaging with ~1 ns pulse-width and <5 μm source size. In this configuration, a wire x-pinch load was driven by the return current and imaged through TXD using 8 keV backlighting from a laser-cut x-pinch. Moiré images with high spatial resolution were recorded, however, phase retrieval was not accomplished due to experimental and data analysis tool limitations [12].

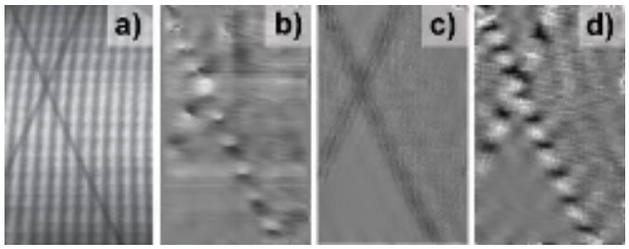

FIG. 7. Images from a 25 μm diameter copper wire x-pinch driven by GenASIS return current. a) Moiré retrieved with TXD backlight by Cu K_α emission from a copper laser-cut foil x-pinch driven by GenASIS main current. TNT retrieval of b) phase, c) attenuation, and d) dark-field.

Figure 7a shows a Moiré image of a copper wire x-pinch (25 μm diameter) with ~4% contrast. In this instance, the Talbot numerical tool enabled the retrieval of the phase map (Figure 7b). Furthermore, TNT also provided attenuation (Figure 7c) and dark-field (Figure 7d) maps. Which were obtained from a single Moiré deflectometry image. The phase image contains electron density gradient information is limited by the system spatial resolution (>2 μm) in the vertical direction and in the horizontal direction it is limited to small "slices" along the wire determined by the Moiré fringe period. It is worth noting that, since the x-pinch load is over-massed (cross-point volume is too large to achieve optimal energy coupling at peak current), maximum wire compression through the Lorentz force is not predicted. For such loads, plasma self-emission is not expected to be bright or localized [38] and thus, it should not decrease Moiré fringe contrast significantly.

The attenuation image shown in Figure 7c, allows for core wire expansion measurement, which confirmed the previously calculated value of 58 and 59 ± 2 μm for each wire [12]. The measurement was also limited by system spatial resolution, determined by object magnification in addition to image plate characteristics and scanning parameters. The most important feature recovered from this image is the lower density plasma that surrounds the dense core. The diameter of this lower density plasma was measured at 135 ± 48 μm, hence, the low-density material has a thickness of ~39 μm. While local electron density retrieval is yet to be performed, valuable information can be inferred from attenuation image analysis. At 8 keV probing energy, the surrounding low-density material transmits ~89%, while the dense core transmits ~80%. Combined with spectral analysis, density and temperature could be inferred. Furthermore, the attenuation image presents refraction enhancement features which can be useful in plasma characterization. However, care must be taken when analyzing refraction enhancement signals as these are further limited by system spatial resolution.

While alternative x-ray imaging methods could provide similar propagation-based x-ray images, TXD diagnostics also provide dark-field maps, as shown in Figure 7d, which is a unique feature to Moiré deflectometry. In similarity to the phase map, small-angle scattering information is limited by spatial resolution along the detection axis and by fringe period in the orthogonal direction. Notably, to the authors knowledge, this is the first time the experimental x-ray dark-field image of a dense plasma load has been recorded. Small-angle scattering is produced by object features smaller than the grating period (few microns in this case), which deviate the x-ray probing beam, altering Moiré fringe contrast. Therefore, dark-field images can provide sub-resolution information through Moiré fringe visibility measurements. Further data analysis of the dark-field image is underway.

IV. SUMMARY

Refraction-based x-ray imaging diagnostic capabilities have been improved through the implementation of a monochromatic TXD platform for the MTW laser. To increase electron density retrieval accuracy, x-ray backlighter targets and laser parameters were investigated to optimize Moiré fringe contrast and spatial resolution. It was found that monochromatic TXD is highly sensitive to line-of-sight misalignments and thus, x-ray backlighter target orientation and location must comply with the multilayer mirror angular requirements. TXD diagnostic data postprocessing capabilities have been improved by the TIA code. In particular, the TNT tool delivers phase, attenuation, and dark-field maps from Moiré images with added features that mitigate x-ray backlighter background and allow for flexible reference image input. A plastic rod was imaged through monochromatic TXD. The x-ray refraction profile obtained with TNT matched simulated data. Similarly, an expanding x-pinch was diagnosed with TXD, and Moiré images were postprocessed with TNT. The retrieved images enabled measurements of core expansion diameter and lower density material thickness. X-ray transmission images made evident the presence of a denser core which is surrounded by low-density plasma. The results here presented constitute important advances in Talbot-Lau imaging diagnostic capabilities. Most importantly, these findings will help guide additional

improvements required for accurate characterization of HEDP experiments through TXD diagnostics.

V. ACKNOWLEDGMENTS

This work was supported by the NNSA Grant Nos. HEDLP DE-NA0003882 and DE-NA0003842. The authors would like to thank LLE science and engineering staff for their support. A.C. and V.B. acknowledge the Conseil Régional Aquitaine (project INTALAX), and the Agence Nationale de la Recherche (ANR-10-IDEX-03-02, ANR-15-CE30-0011) for their funding support.

VI. REFERENCES

[1] R. P. Drake, "A journey through high-energy-density physics," *Nuclear Fusion*, vol. 59, no. 3, p. 035001, 2018.

[2] F. Pfeiffer, T. Weitkamp, O. Bunk, and C. David, "Phase retrieval and differential phase-contrast imaging with low-brilliance X-ray sources," *Nat Phys*, vol. 2, no. 4, pp. 258–261, Mar. 2006, doi: 10.1038/nphys265.

[3] A. Momose *et al.*, "Phase tomography by X-ray talbot interferometry for biological imaging," *Japanese Journal of Applied Physics, Part 1: Regular Papers and Short Notes and Review Papers*, vol. 45, no. 6 A, pp. 5254–5262, 2006, doi: 10.1143/JJAP.45.5254.

[4] D. Stutman and M. Finkenthal, "Talbot-Lau x-ray interferometry for high energy density plasma diagnostic.," *Rev Sci Instrum*, vol. 82, no. 11, p. 113508, Nov. 2011, doi: 10.1063/1.3660808.

[5] M. P. Valdivia, D. Stutman, and M. Finkenthal, "Moire deflectometry using the Talbot-Lau interferometer as refraction diagnostic for High Energy Density plasmas at energies below 10 keV," *Review of Scientific Instruments*, vol. 85, no. 7, p. 073702, 2014, doi: 10.1063/1.4885467.

[6] M. P. Valdivia *et al.*, "Talbot-Lau X-ray Deflectometer: Refraction-based HEDP imaging diagnostic," *Review of Scientific Instruments*, vol. 92, no. Proceedings of the 23rd Topical Conference on High-Temperature Plasma Diagnostics, p. 065110, 2021, doi: 10.1063/5.0043655.

[7] O. Kafri and I. Glatt, "Moire Deflectometry: A Ray Deflection Approach To Optical Testing," *Optical Engineering*, vol. 24, no. 6, p. 246944, 1985, doi: https://doi.org/10.1117/12.7973607.

[8] M. P. Valdivia, D. Stutman, and M. Finkenthal, "Single-shot Z eff dense plasma diagnostic through simultaneous refraction and attenuation measurements with a Talbot – Lau x-ray moiré deflectometer," *Appl Opt.*, vol. 54, no. 10, pp. 2577–2583, 2015, doi: 10.1364/AO.54.002577.

[9] M. P. Valdivia *et al.*, "Talbot – Lau x-ray deflectometry phase-retrieval methods for electron density diagnostics in high-energy density experiments," *Appl Opt*, vol. 57, no. 2, pp. 13–15, 2018.

[10] M. P. Valdivia *et al.*, "An x-ray backlit Talbot-Lau deflectometer for high-energy-density electron density diagnostics," *Review of Scientific Instruments*, vol. 87, no. 2, p. 023505, 2016, doi: 10.1063/1.4941441.

[11] M. P. Valdivia *et al.*, "Implementation of a Talbot – Lau x-ray deflectometer diagnostic platform for the OMEGA EP laser," *Rev. Sci. Instrum.*, vol. 91, no. 2, p. 023511, 2020, doi: 10.1063/1.5123919.

[12] M. P. Valdivia, G. W. Collins IV, F. Conti, and F. N. Beg, "Wire, hybrid, and laser-cut X-pinches as Talbot-Lau backlighters for electron density diagnostics," *Plasma Phys Control Fusion*, vol. 64, no. 3, 2022, doi: 10.1088/1361-6587/ac4b95.

[13] M. Vescovi, M. P. Valdivia, F. Veloso, D. Stutman, and M. Favre, "Implementation of Talbot–Lau x-ray deflectometry in the pulsed power environment using a copper X-pinch backlighter," *J Appl Phys*, vol. 127, no. 20, p. 203301, 2020, doi: 10.1063/5.0001910.

[14] V. Bouffetier *et al.*, "Proof-of-concept Talbot – Lau x-ray interferometry laser-driven K-alpha source," *Appl Opt*, vol. 59, no. 27, pp. 8380–8387, 2020.

[15] M. P. Valdivia *et al.*, "X-ray backlighter requirements for refraction-based electron density diagnostics through Talbot-Lau deflectometry," *Rev. Sci. Instrum.*, vol. 89, no. 10G127, pp. 138–145, 2018, doi: 10.1063/1.5039342.

[16] I. A. Begishev *et al.*, "Advanced laser development and plasma-physics studies on the multiterawatt laser," *Appl Opt*, vol. 60, no. 36, p. 11104, 2021, doi: 10.1364/ao.443548.

[17] R. Bott, S. Haas, D. Madden, R. Ueda, U. Eshaq, Y. Collins, G. Gunasekera, K. Mariscal, D. Peebles, J. Beg, F. Mazarakis, M. Struve, K. Sharpe, "250 kA compact linear transformer driver for wire array z-pinch loads," *Physical Review Special Topics - Accelerators and Beams*, vol. 14, no. 5, pp. 1–8, May 2011, doi: 10.1103/PhysRevSTAB.14.050401.

[18] G. Perez-Callejo *et al.*, "TIA: A forward model and analyzer for Talbot interferometry experiments of dense plasmas," *Phys Plasmas*, vol. 043901, no. April, p. 04391, 2022, doi: 10.1063/5.0085822.

[19] C. Stoeckl *et al.*, "Monochromatic backlighting of direct-drive cryogenic DT implosions on OMEGA," *Phys Plasmas*, vol. 24, no. 5, 2017, doi: 10.1063/1.4977918.

[20] S. A. Pikuz *et al.*, "High-luminosity monochromatic x-ray backlighting using an incoherent plasma source to study extremely dense plasmas (invited)," *Review of Scientific Instruments*, vol. 68, no. 1, p. 740, 1997, doi: 10.1063/1.1147689.

[21] Y. Aglitskiy *et al.*, "High resolution monochromatic X-ray imaging system based on spherically bent crystals," *The fourth international conference on dense z-pinches*, vol. 37, no. 22, pp. 437–441, 1997, doi: 10.1063/1.53824.

[22] D. B. Sinars *et al.*, "Monochromatic x-ray backlighting of wire-array z-pinch plasmas using spherically bent quartz crystals," *Review of Scientific Instruments*, vol. 74, no. 3, p. 2202, 2003, doi: 10.1063/1.1537853.

[23] J. A. Koch *et al.*, "High-energy x-ray microscopy techniques for laser-fusion plasma research at the National Ignition Facility," *Appl Opt*, vol. 37, no. 10, p. 1784, 1998, doi: 10.1364/ao.37.001784.

[24] X. Cheng, B. Tan, J. Cheng, and J. Mu, "Laterally graded multilayer as x-ray mirror for the laser-induced plasma x- ray sources," vol. 1038604, no. August 2017, 2019, doi: 10.1117/12.2272376.

[25] B. Jones *et al.*, "Design of a multilayer mirror monochromatic x-ray imager for the accelerator," *Review of scientific instruments*, vol. 75, no. 10, pp. 4029–4032, 2004, doi: 10.1063/1.1789257.

[26] L. P. Jones B, Deeney C, Coverdale CA, Meyer CJ, "Multilayer mirror monochromatic selfemission x-ray

imaging on the Z accelerator," *Review of Scientific Instruments*, vol. 77, no. 10E316, 2006.

[27] H. S. Park *et al.*, "High-resolution 17–75 keV backlighters for high energy density experiments," *Phys Plasmas*, vol. 15, no. 7, p. 072705, 2008, doi: 10.1063/1.2957918.

[28] I. H. Hutchinson, "Principles of Plasma Diagnostics: Second Edition," *Plasma Phys Control Fusion*, vol. 44, no. 12, p. 2603, Nov. 2002, doi: 10.1088/0741-3335/44/12/701.

[29] R. F. Smith *et al.*, "Picosecond x-ray laser interferometry of dense plasmas," *Phys Rev Lett*, vol. 89, no. 6, pp. 065004/1-065004/4, 2002, doi: 10.1103/PhysRevLett.89.065004.

[30] J. Filevich *et al.*, "Picosecond-resolution soft-x-ray laser plasma interferometry.," *Appl Opt*, vol. 43, no. 19, pp. 3938–46, Jul. 2004.

[31] J. Grava *et al.*, "Dynamics of a dense laboratory plasma jet investigated using soft x-ray laser interferometry," *Phys Rev E Stat Nonlin Soft Matter Phys*, vol. 78, no. 1, pp. 1–9, 2008, doi: 10.1103/PhysRevE.78.016403.

[32] T. Weitkamp, "XWFP: an x-ray wavefront propagation software package for the IDL computer language," in *Advances in Computational Methods for X-Ray and Neutron Optics*, Oct. 2004, vol. 5536, no. October 2004, pp. 181–189. doi: 10.1117/12.569642.

[33] M. Hipp, "User Manual for IDEA 1.7," vol. 57, no. July, 2003.

[34] F. Pfeiffer *et al.*, "Hard-X-ray dark-field imaging using a grating interferometer.," *Nat Mater*, vol. 7, no. 2, pp. 134–7, Feb. 2008, doi: 10.1038/nmat2096.

[35] T. A. Shelkovenko *et al.*, "Hybrid X-pinch with conical electrodes," *Phys Plasmas*, vol. 17, no. 11, p. 112707, 2010, doi: 10.1063/1.3504226.

[36] G. W. Collins *et al.*, "Investigation into the dynamics of laser-cut foil X-pinches and their potential use for high repetition rate operation," *Appl Phys Lett*, vol. 105, no. 2, p. 024101, 2014, doi: 10.1063/1.4889748.

[37] G. W. Collins *et al.*, "Direct comparison of wire, foil, and hybrid X-pinches on a 200 kA, 150 ns current driver," *J. Appl. Phys.*, vol. 129, no. 7, 2021, doi: 10.1063/5.0035587.

[38] S. A. Pikuz, T. A. Shelkovenko, and D. A. Hammer, "X-pinch. Part I," *Plasma Physics Reports*, vol. 41, no. 4, pp. 291–342, 2015, doi: 10.1134/S1063780X15040054.

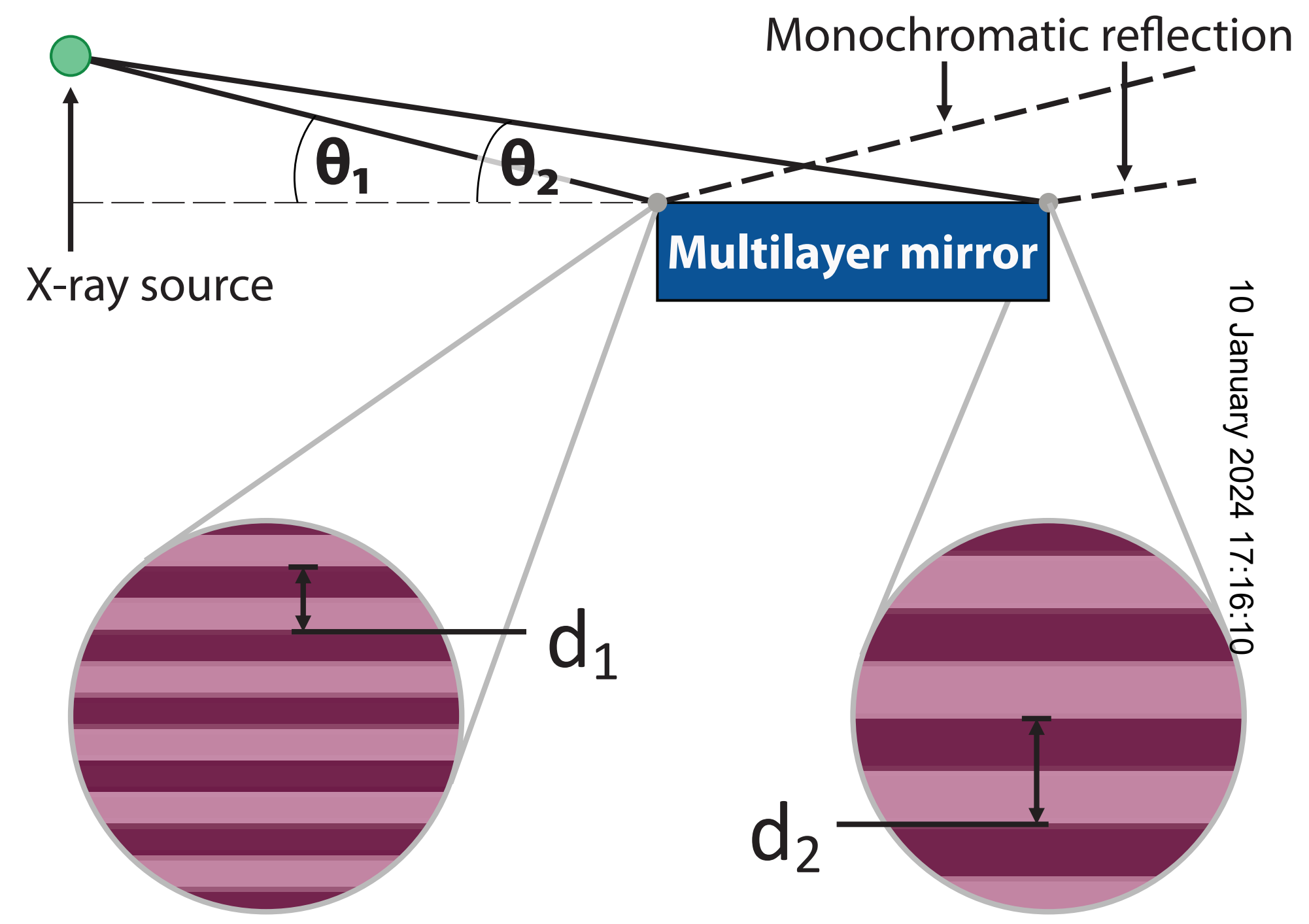
Monochromatic reflection
θ1
θ2
X-ray source
Multilayer mirror
d1
d2
10 January 2024 17:16:10

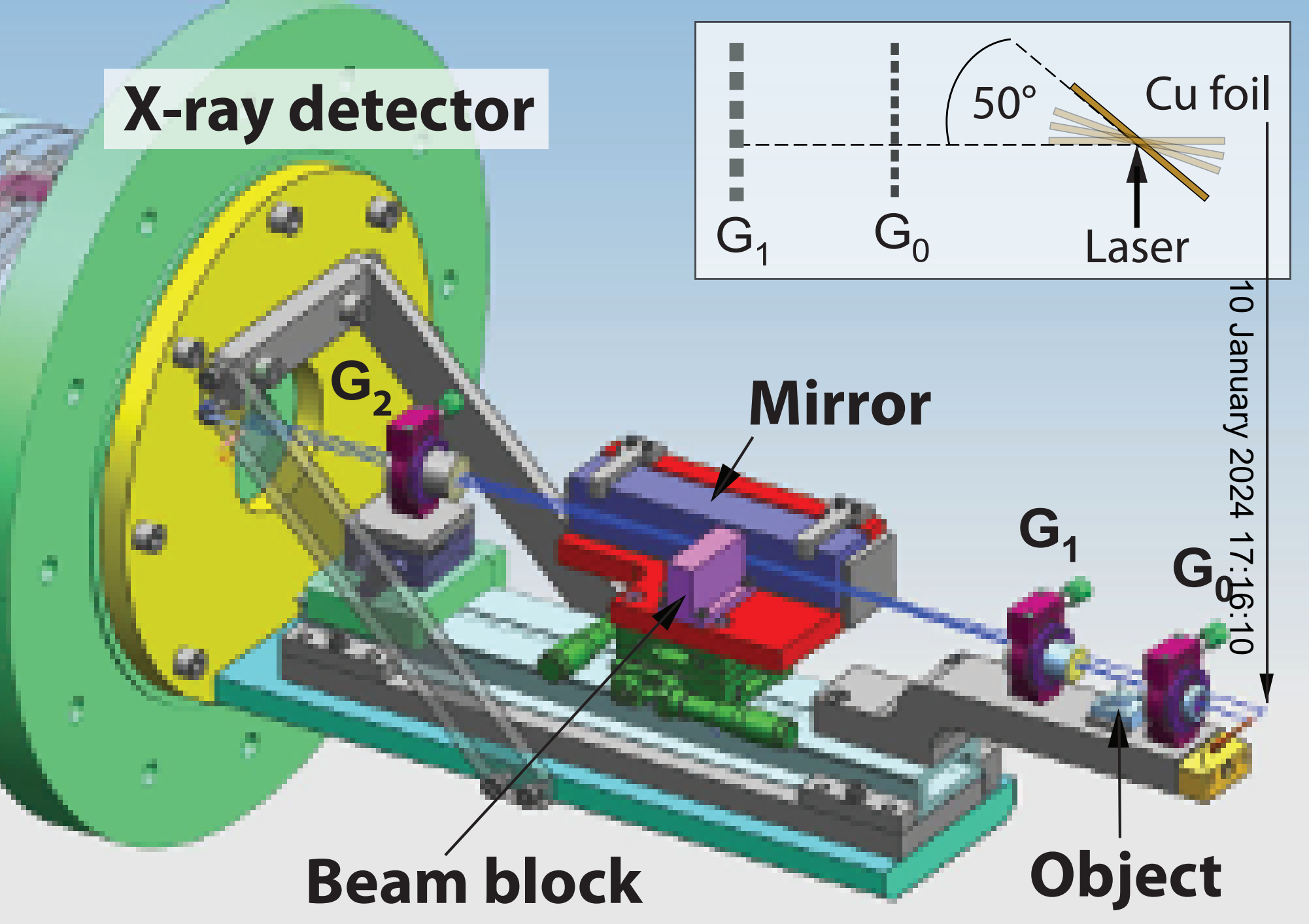
X-ray detector
50°
Cu foil
G1
G0
Laser
10 January 2024 17:16:10
G2
Mirror
G1
G0
Beam block
Object

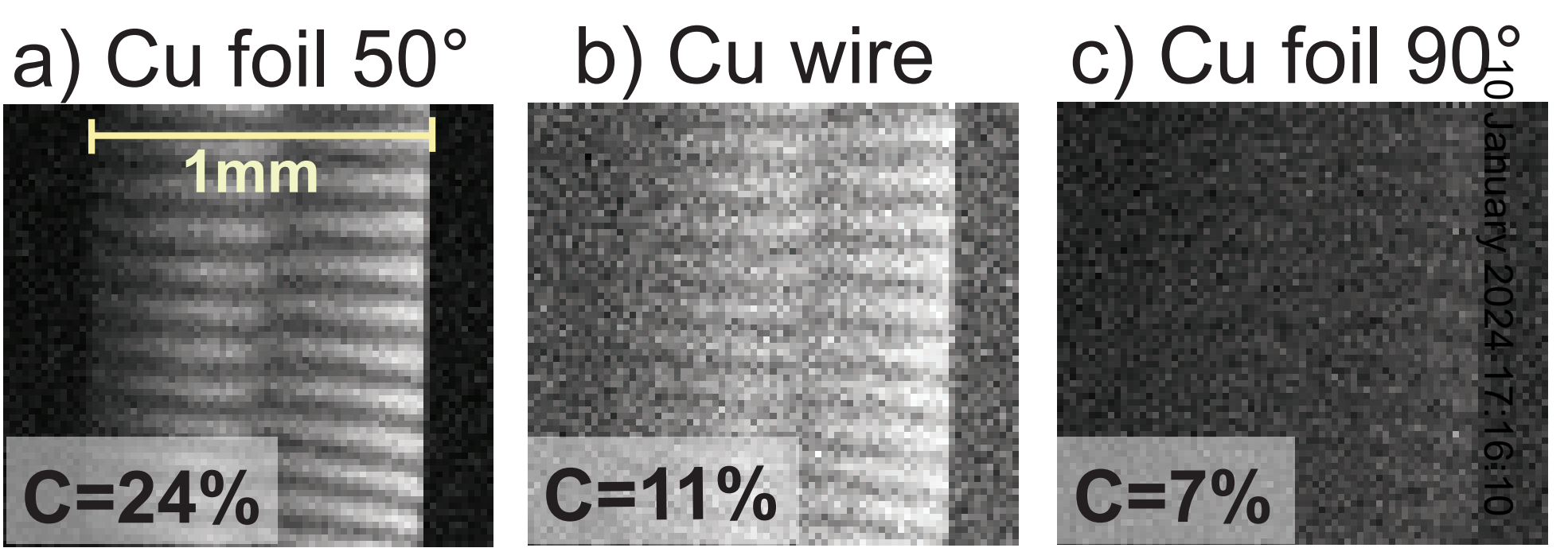
a) Cu foil 50°
b) Cu wire
c) Cu foil 90°
1mm
C=24%
C=11%
C=7%
10 January 2024 17:16:10

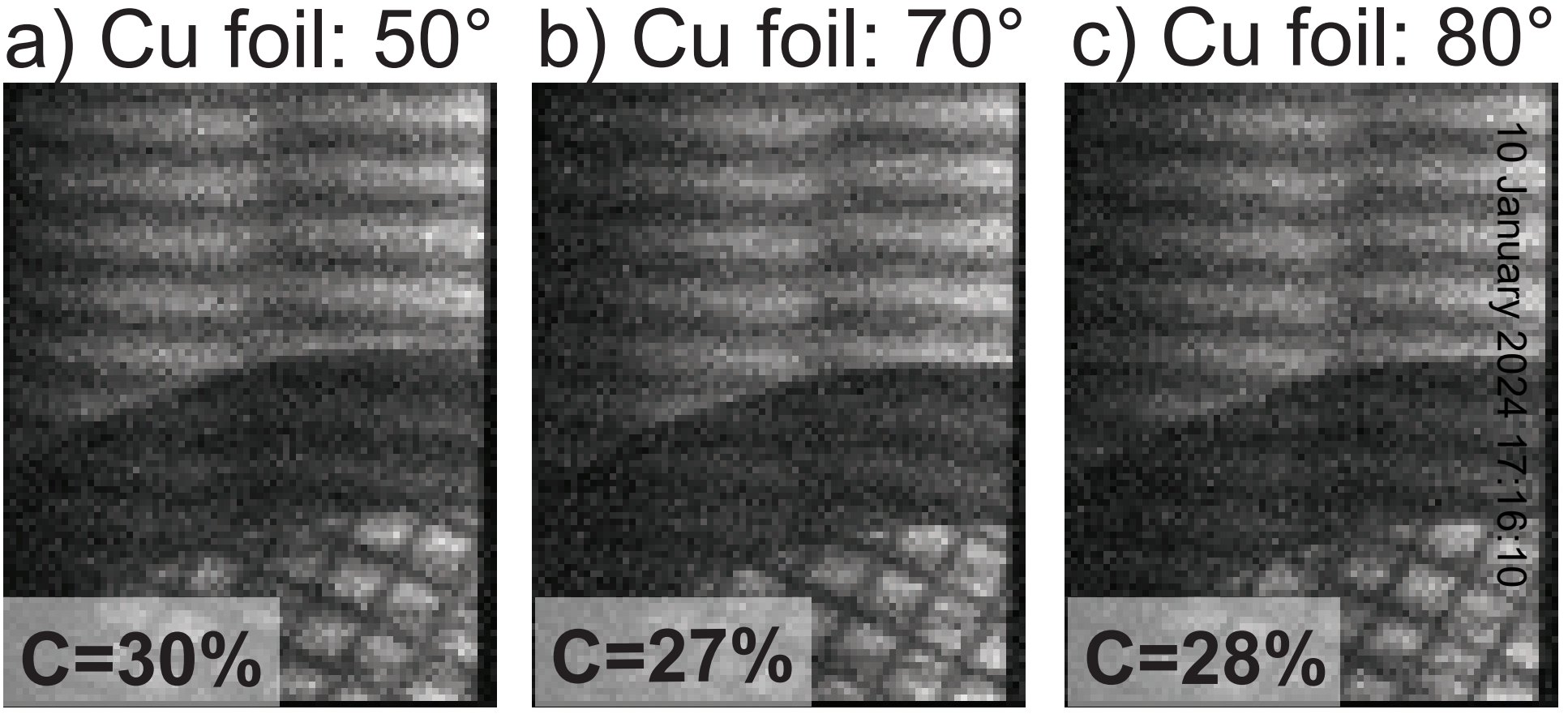
a) Cu foil: 50°
b) Cu foil: 70°
c) Cu foil: 80°
C=30%
C=27%
C=28%
10 January 2024 17:16:10

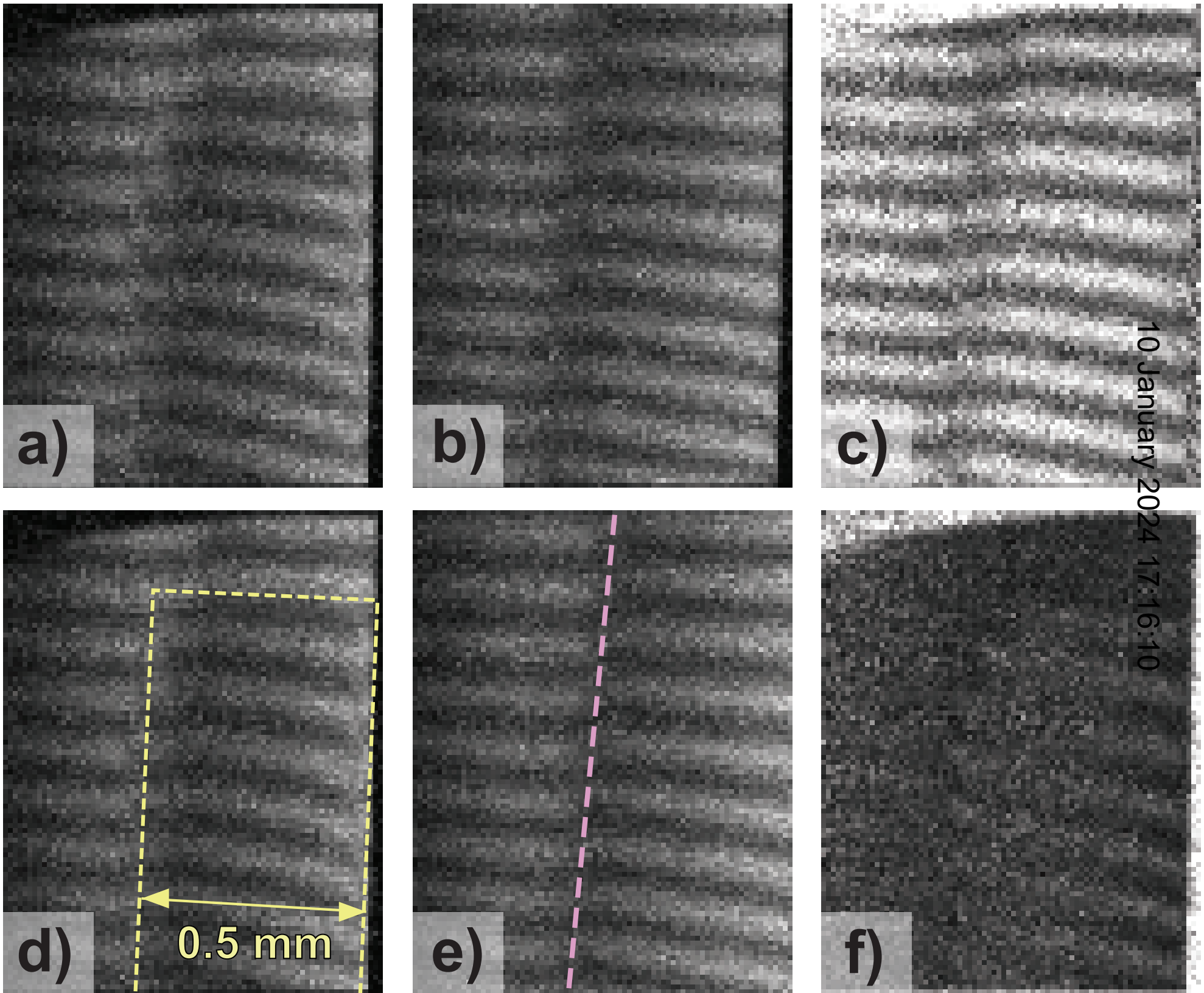
a)
b)
c)
10 January 2024 17:16:10
d)
0.5 mm
e)
f)

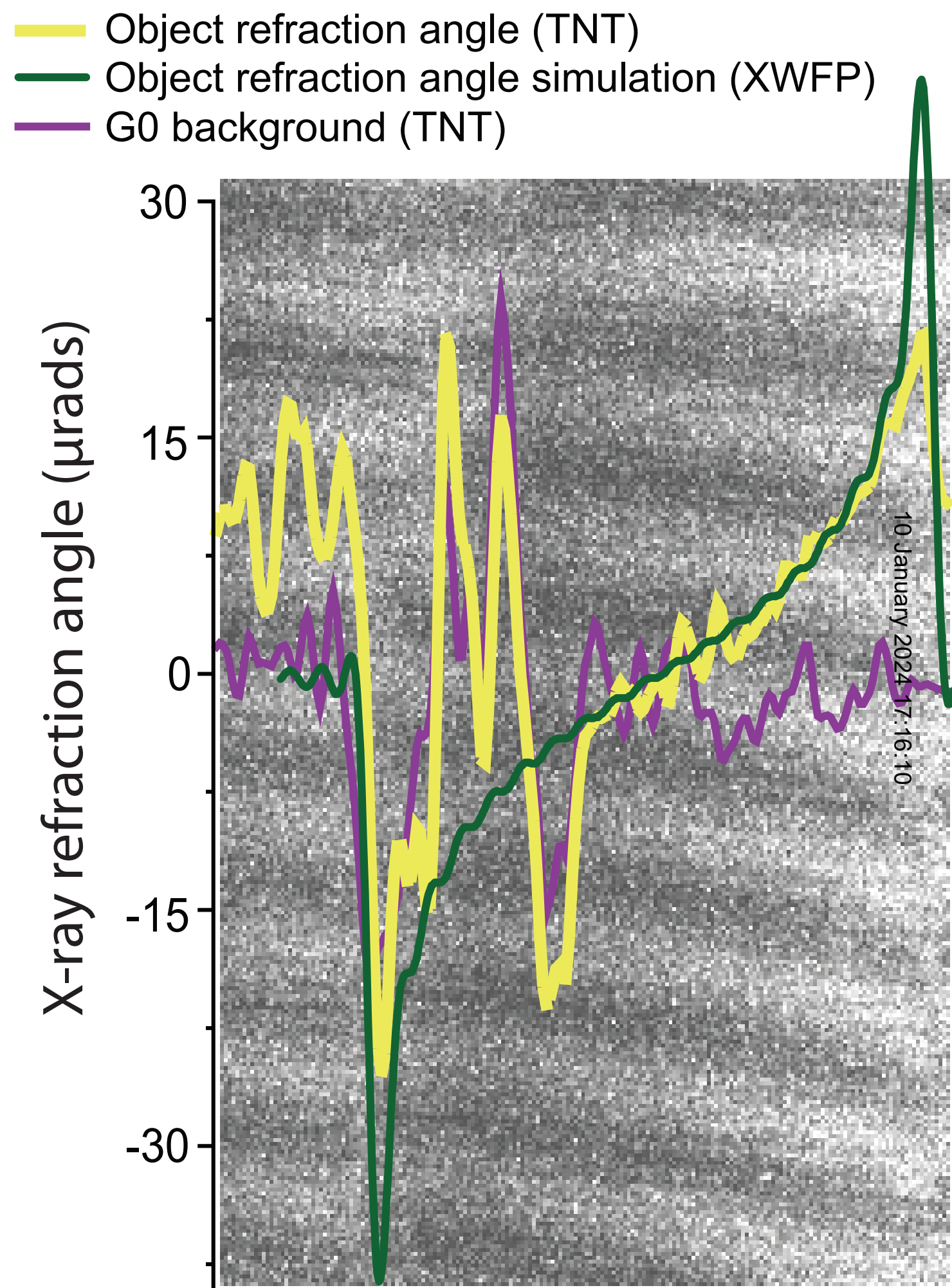
Object refraction angle (TNT)
Object refraction angle simulation (XWFP)
G0 background (TNT)
X-ray refraction angle (µrads)
30
15
0
-15
-30
10 January 2024 17:16:10

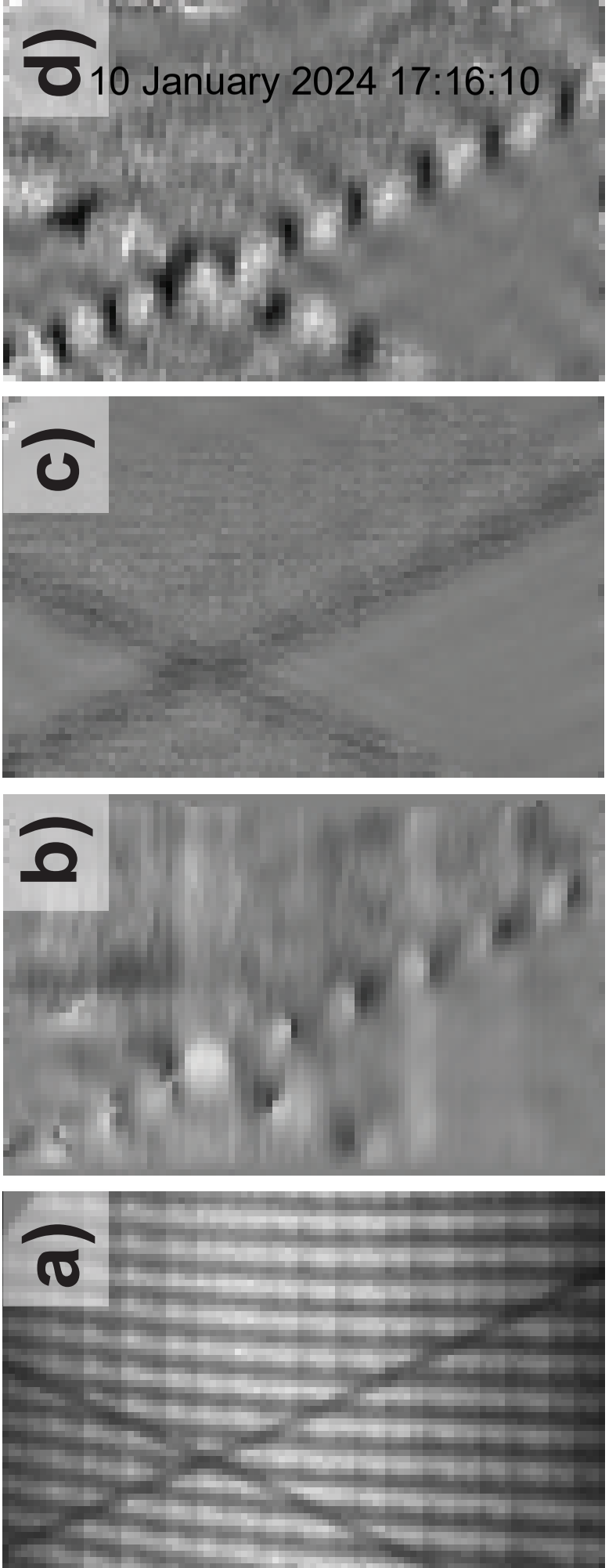
d)
10 January 2024 17:16:10
c)
b)
a)